

Assessment of negative and positive CO₂ emissions on global warming metrics using an ensemble of Earth system model simulations

5 Negar Vakilifard¹, Richard G. Williams², Philip B. Holden¹, Katherine Turner^{2,3}, Neil R. Edwards^{1,4}, and David J. Beerling⁵

¹Environment, Earth and Ecosystems, The Open University, Milton Keynes, UK

²Department of Earth, Ocean and Ecological Sciences, School of Environmental Sciences, University of
10 Liverpool, Liverpool, UK

³Leverhulme Research Centre for Functional Materials Design, Liverpool, UK

⁴Cambridge Centre for Energy, Environment and Natural Resource Governance, University of
Cambridge, Cambridge, UK

⁵Leverhulme Centre for Climate Change Mitigation, School of Biosciences, University of Sheffield,
15 Sheffield, UK

Correspondence to: Negar Vakilifard (negar.vakilifard@open.ac.uk)

Keywords: effective TCRE, carbon-cycle feedback, climate feedback, ocean heat uptake, hysteresis of
the Earth system, negative emissions, effective zero emissions commitment, uncertainty in the Earth
20 system's feedbacks

Abstract

The benefits of implementing negative emission technologies on the global warming response to cumulative carbon emissions until year 2420 are assessed following the shared socioeconomic pathways (SSP)1-2.6, the sustainable development scenario, with a comprehensive set of intermediate complexity Earth system model integrations. Model integrations include 86 different model realisations covering a wide range of plausible climate states. The global warming response is assessed in terms of two key climate metrics: the effective transient climate response to cumulative CO₂ emissions (eTCRE), measuring the surface warming response to cumulative carbon emissions and associated non-CO₂ forcing, and the effective zero emissions commitment (eZEC), measuring the extent of any continued warming after net zero CO₂ emissions is reached. The TCRE is approximated from eTCRE by removing the contributions of non-CO₂ forcing of 2.2 K EgC⁻¹ (median value) (with a 10-90 % range of 1.75 to 3.13 K EgC⁻¹ in 2100). During the positive emission phase, the eTCRE decreases from 2.71 (2.0 to 3.65) to 2.61 (1.91 to 3.62) K EgC⁻¹ due to a weakening in radiative forcing with an increase in atmospheric carbon, which is partly opposed by an increasing fraction of the radiative forcing warming the surface as the ocean stratifies. During the net negative and zero emission phases, a progressive reduction of the eTCRE to 2.0 (1.39 to 2.96) K EgC⁻¹ is driven by the reducing airborne fraction as CO₂ is drawn down mainly by the ocean. The model uncertainty in the slopes of warming versus cumulative CO₂ emissions varies from being controlled by the radiative feedback parameter during positive emissions to being affected by carbon-cycle parameters during net negative emissions, consistent with the drivers of uncertainty diagnosed from the coefficient of variation of the contributions in the eTCRE framework. The continued warming after CO₂ emissions cease and remain at zero gives a model mean eZEC of -0.03 K at 25 years which decreases in time to -0.21 K at 90 years after emissions cease. However, there is a spread in the ensemble with a temperature overshoot occurring in 20 % of the ensemble members at year 25. If net negative emissions are included, there is a reduction in atmospheric CO₂ and there is a decrease in temperature overshoot, so that the eZEC is positive in only 5 % of the ensemble members. Hence, incorporating negative emissions enhances the ability to meet climate targets and avoid risk of continued warming after net zero is reached.

1 Introduction

50 There is an increasing need to adopt negative emission technologies (Luderer et al., 2013; Rogelj et al., 2015; Beerling et al., 2020) to enhance the chance of meeting the Paris climate agreement target (UNFCCC, 2015) to hold global warming well below 2 °C with an ambition of 1.5 °C given the ongoing growth in greenhouse gas concentrations (Boucher et al., 2012; Jeltsch-Thömmes et al., 2020). For a 1.5 °C target, there is 66 % chance of meeting this target only if post-2019 cumulative carbon emissions are limited to less than ~ 400 GtCO₂ (IPCC, 55 2021). Two climate metrics of transient climate response to cumulative CO₂ emissions (TCRE) and zero emissions commitment (ZEC) are essential to determine how much carbon may be emitted while remaining within the warming target.

The remaining carbon budget is inversely proportional to TCRE, the increase in the mean-global surface air temperature relative to cumulative CO₂ emission (Matthews et al., 2009; Zickfeld et al., 2012; IPCC, 2013; Gillett et al., 2013; Zickfeld et al., 2013; Friedlingstein et al., 2014; Matthews et al., 2017). Climate model projections 60 reveal a simple near-linear relationship between the global surface air temperature change and cumulative CO₂ emissions between 0 and ~ 2000 PgC (MacDougall, 2016). However, despite a similar linear dependence, there is a wide inter-model range in TCRE values (Williams et al., 2017; Spafford and MacDougall, 2020), varying from 1.4 to 2.5 K TtC⁻¹ in intermediate-complexity Earth system models (Eby et al., 2013), 0.8 to 2.4 K TtC⁻¹ in full- 65 complexity Earth system models (Matthews et al., 2018), and 0.7 to 2.0 K TtC⁻¹ (90 % confidence interval) in observationally-constrained TCRE estimates from a 15-member CMIP5 ensemble (Gillett et al., 2013).

For the case of radiative forcing exclusively from atmospheric CO₂, the TCRE can be related to the dependence of the global mean temperature on the radiative forcing, the dependence of the radiative forcing on the atmospheric CO₂ and the airborne fraction (Sect. 2; Williams et al., 2016; Ehlert et al., 2017; Katavouta et al., 70 2018; Williams et al., 2020). Applying this framework to 7 CMIP5 and 9 CMIP6 models following a 1 % annual increase in atmospheric CO₂, the TCRE is affected by a large inter-model spread in the climate feedback parameter for CMIP6 (Williams et al., 2020) as well as by a larger inter-model spread in the land carbon system for CMIP5 (Jones and Friedlingstein, 2020). The inclusion of non-CO₂ radiative forcing alters the relationship between emissions and surface warming through both direct warming and carbon feedback effects (Tokarska et al., 2018). 75 For the more realistic case including non-CO₂ radiative forcing contributions, the TCRE may be estimated by approximately removing the warming linked to non-CO₂ radiative forcing (Matthews et al., 2021). Alternatively, an effective TCRE (eTCRE) may be defined to include non-CO₂ warming and the non-CO₂ radiative forcing (Williams et al., 2016; Williams et al., 2017).

The climate response after net zero emissions is an important climate metric, encapsulated in the zero emissions commitment (ZEC) given by the mean surface air temperature change after CO₂ emissions cease (Hare and Meinshausen, 2006; Matthews and Caldeira, 2008, Froelicher and Paynter, 2015; MacDougall et al., 2020). Quantification of the ZEC is critical for calculating the remaining carbon budget. Whether there is continued surface warming depends on a competition between a cooling effect from the reduction of the radiative forcing from atmospheric CO₂ as carbon is taken up by the ocean and terrestrial biosphere, versus a surface warming effect from a decline in the heat uptake by the ocean interior (Williams et al., 2017b). In an analysis of Earth system model responses to idealised CO₂-only forcing, MacDougall et al. (2020) found a multi-model mean ZEC close to zero, with a wide spread in continued warming and cooling responses from individual models. Matthews and Zickfeld (2012) previously analysed the ZEC in the context of a realistic scenario by including contributions from non-CO₂ forcings, but these authors did not address uncertainty. We address this gap by applying a perturbed physics ensemble to an experiment which includes non-CO₂ forcing within the framework of a strong mitigation scenario as is most appropriate for negative emissions.

Here we examine these two climate metrics, the TCRE and the ZEC following the shared socioeconomic pathway (SSP) 1-2.6 scenario, which combines the realistic socio-economic conditions for sustainable development with the high mitigation RCP 2.6 scenario assuming large-scale employment of a range of greenhouse gas mitigation technologies and strategies. Our analysis is based on simulations with the intermediate complexity Earth system model GENIE-1. The use of intermediate complexity enables us to (i) quantify uncertainties through an ensemble consisting of 86 members that provide a wide range of plausible climate states and (ii) explore long timescales, in both the historical and future periods. The pre-industrial baseline is chosen as 850 CE (Eby et al., 2013) rather than 1850 CE to account for both land use change and fossil fuel CO₂ emissions occurring before 1850 CE. We, however, acknowledge that the reconstructions of land use change emissions for the periods prior to about 1800 have been based on the prior estimates of population, mortality rate and land use assumptions and hold large uncertainties (Koch et al., 2019). The model was spun up to pre-industrial climate and integrated from years 850 to 2420 CE, extending several centuries after the emissions cease to reveal whether there is continued warming and to quantify the effectiveness of negative emission applications. The TCRE analysis follows an eTCRE framework (Williams et al., 2016; Ehlert et al., 2017; Katavouta et al., 2018; Williams et al., 2020) and compares with a correlation analysis between the varied model parameters and the slopes of change in temperature versus cumulative emissions. The effective ZEC (eZEC) analysis addresses the response of the ensemble during periods of net zero carbon emissions but continued non-CO₂ forcing following the SSP 1-2.6 scenario.

In this study, the theoretical framework used to interpret the TCRE is set out including defining its thermal, radiative and carbon contributions (Sect. 2). The model methodology using the intermediate complexity Earth system model GENIE-1 is described (Sect. 3) and the model responses including the spread in ensemble responses (Sect. 4). The controls of the climate responses as defined by the two climate metrics, the effective TCRE and effective ZEC, are explored including outlining the asymmetrical response to positive and negative emissions (Sect. 5). Finally, the implications of study are summarised including the benefits from implementing negative emissions (Sect. 6).

2 Theoretical framework

We first introduce the framework under the assumption of only CO₂ forcing. A climate metric TCRE (in K EgC⁻¹) is defined as the surface warming response to cumulative CO₂ emissions

$$TCRE = \frac{\Delta T(t)}{I_{em}(t)}, \quad (1)$$

where Δ is the change since year 850 CE, $\Delta T(t)$ is the global mean change in surface air temperature (in K) and $I_{em}(t)$ is the cumulative CO₂ emissions (in PgC) from the sum of fossil fuel emissions and land use changes.

The TCRE may be viewed as a product of two terms, the change in global mean air temperature divided by the change in the atmospheric carbon inventory, $\Delta T(t)/\Delta I_{atmos}(t)$, and the airborne fraction, $\Delta I_{atmos}(t)/I_{em}(t)$, given by the change in the atmospheric carbon inventory (in PgC) divided by the cumulative CO₂ emissions (Matthews et al., 2009; Solomon et al., 2009; Gillett et al., 2013; MacDougall, 2016) such that

$$TCRE \equiv \frac{\Delta T(t)}{I_{em}(t)} = \left(\frac{\Delta T(t)}{\Delta I_{atmos}(t)} \right) \left(\frac{\Delta I_{atmos}(t)}{I_{em}(t)} \right), \quad (2)$$

where $\Delta T(t)/\Delta I_{atmos}(t)$ is related to the transient climate response, defined by the temperature change at the time of doubling of atmospheric CO₂ (Matthews et al., 2009). The TCRE is defined in terms of this surface warming response to CO₂ forcing, usually following a 1 % annual rise in atmospheric CO₂.

Alternatively, the TCRE may be linked to an identity involving a thermal dependence on radiative forcing, defined by the change in temperature divided by the change in radiative forcing, $\Delta T(t)$ (in Wm⁻²), and the radiative forcing dependence on CO₂ emissions, defined by the change in radiative forcing divided by the cumulative CO₂ emissions (Goodwin et al., 2015; Williams et al., 2016; Williams et al., 2017) such that

$$TCRE \equiv \frac{\Delta T(t)}{I_{em}(t)} = \left(\frac{\Delta T(t)}{\Delta F(t)} \right) \left(\frac{\Delta F(t)}{I_{em}(t)} \right). \quad (3)$$

These two viewpoints can be rationalized by rewriting the radiative forcing dependence to CO₂ emissions in Eq. 3 in terms of the radiative forcing dependence on atmospheric CO₂ and the airborne fraction (Ehlert et al., 2017; Katavouta et al., 2018; Williams et al., 2020).

135 The TCRE is then defined by the product of the thermal dependence, the radiative dependence between radiative forcing and atmospheric carbon, and the carbon dependence involving the airborne fraction:

$$TCRE \equiv \frac{\Delta T(t)}{I_{em}(t)} = \underbrace{\left(\frac{\Delta T(t)}{\Delta F(t)}\right)}_{thermal} \underbrace{\left(\frac{\Delta F(t)}{\Delta I_{atmos}(t)}\right)}_{radiative} \underbrace{\left(\frac{\Delta I_{atmos}(t)}{I_{em}(t)}\right)}_{carbon}. \quad (4)$$

The thermal response may be further understood from an empirical global radiative balance (Gregory et al., 2004; Forster et al., 2013). The increase in radiative forcing, $\Delta F(t)$, drives an increase in planetary heat uptake, $N(t)$ (in Wm⁻²), plus a radiative response, which is assumed to be equivalent to the product of the increase in
140 global mean surface air temperature, $\Delta T(t)$, and the climate feedback parameter, $\lambda(t)$ (in K⁻¹ Wm⁻²):

$$\underbrace{\Delta F(t)}_{radiative\ forcing} = \underbrace{N(t)}_{heat\ uptake} + \underbrace{\lambda(t)\Delta T(t)}_{radiative\ response}. \quad (5)$$

The thermal dependence in Eq. 4 given by the dependence of surface warming on radiative forcing, $\Delta T(t)/\Delta F(t)$, is then given by the product of the inverse of the climate feedback, $\lambda^{-1}(t)$, and the planetary heat uptake divided by the radiative forcing, $N(t)/\Delta F(t)$,

$$\frac{\Delta T(t)}{\Delta F(t)} = \frac{1}{\lambda(t)} \left(1 - \frac{N(t)}{\Delta F(t)}\right), \quad (6)$$

145 where $1 - N(t)/\Delta F(t)$ represents the fraction of the radiative forcing that is lost to space and may be viewed as effectively equivalent to the fraction of the radiative forcing that warms the surface rather than the ocean interior.

The carbon dependence in Eq. 4 involving the airborne fraction, $\Delta I_{atmos}(t)/I_{em}(t)$, is related to the changes in the ocean-borne, land-borne and sediment-borne fractions (Jones et al., 2013),

$$\frac{\Delta I_{atmos}(t)}{I_{em}(t)} = 1 - \left(\frac{\Delta I_{ocean}(t)}{I_{em}(t)} + \frac{\Delta I_{land}(t)}{I_{em}(t)} + \frac{\Delta I_{sediment}(t)}{I_{em}(t)}\right), \quad (7)$$

where the changes in the ocean, land and sediment inventories are denoted by $\Delta I_{ocean}(t)$, $\Delta I_{land}(t)$ and $\Delta I_{sediment}(t)$ (in PgC), respectively.

150 The TCRE is formally defined in terms of the climate response to cumulative CO₂ emissions following a 1 % annual rise in atmospheric CO₂ (Matthews et al., 2009). As the rise in anthropogenic radiative forcing is currently dominated by the radiative forcing from atmospheric CO₂, the TCRE is a useful climate metric to understand future climate projections. However, in the more realistic framework we apply here, the warming response includes

contributions from non-CO₂ forcing. In such experiments, Matthews et al. (2021) advocate estimating the TCRE
 155 by approximately removing the warming due to the non-CO₂ radiative forcing by multiplying by a
 non-dimensional factor $(1 - f_{nc})$, now explicitly acknowledging that $\Delta T(t)$ is not solely driven by $I_{em}(t)$:

$$TCRE = \frac{\Delta T(t)}{I_{em}(t)}(1 - f_{nc}). \quad (8)$$

Matthews et al. (2021) interpret the non-dimensional factor $(1 - f_{nc})$ to represent the non-CO₂ fraction of
 total anthropogenic forcing where $f_{nc} = (\Delta F(t) - \Delta F_{CO_2}(t))/\Delta F(t)$. This estimation of the TCRE from general
 forcing scenarios assumes that the time- and scenario- independence of the TCRE translates to a general response
 160 independence from radiative forcing elements.

In order to allow for possible changes in the thermal and carbon responses from the non-CO₂ forcing, we
 prefer to define an eTCRE including the effect of the radiative forcing from non-CO₂ and CO₂ radiative
 components using a series of mathematical identities (Williams et al., 2016 and 2017), where

$$eTCRE \equiv \frac{\Delta T(t)}{I_{em}(t)} = \underbrace{\left(\frac{\Delta T(t)}{\Delta F(t)}\right)}_{thermal} \underbrace{\left(\frac{\Delta F(t)}{\Delta F_{CO_2}(t)}\right)}_{radiative\ from\ CO_2\ and\ non-CO_2} \underbrace{\left(\frac{\Delta F_{CO_2}(t)}{\Delta I_{atmos}(t)}\right)}_{carbon} \underbrace{\left(\frac{\Delta I_{atmos}(t)}{I_{em}(t)}\right)}_{carbon}. \quad (9)$$

By including the effect of the non-CO₂ radiative forcing, the eTCRE in Eq. 9 is larger than the TCRE with
 165 non-CO₂ radiative forcing removed in Eq. 8 whenever the positive radiative effect of non-CO₂ greenhouse gases
 exceeds the negative effect from aerosols. Our subsequent model diagnostics focus on evaluating the eTCRE and
 the thermal, radiative and carbon dependences using Eq. 9.

3 GENIE-1 model description and experiment design

Our analysis is based on an Earth system model simulations for SSP1-2.6, the scenario with the least
 170 socioeconomic challenges to adaptation and mitigation of climate change (O'Neill et al., 2017; Riahi et al., 2017)
 which allows large-scale deployment of negative emissions technologies (NETs). Here, we investigate the
 implications of NETs for atmospheric CO₂ removal over 400 years by applying the net negative emissions of
 ~ 156 PgC between the years 2077 to 2250 (Fig. 1a-b).

We employed the global intermediate complexity Earth system model, GENIE-1 (release 2.7.7) (Holden et
 175 al., 2013a), consisting of the 3-D frictional geostrophic ocean model (GOLDSTEIN) ($36^\circ \times 36^\circ$ resolution with 16
 depths levels in the ocean) coupled to the 2-D energy moisture balance model of the atmosphere (EMBM) and a
 thermodynamic-dynamic sea-ice model (Edwards and Marsh, 2005). The land surface module is the dynamic

model of terrestrial carbon and land use change ENTSML (Holden et al., 2013a). Ocean biochemistry, deep-sea
sediments and rock weathering are modelled by BIOGEM (Ridgwell et al., 2007), SEDGEM ($36^\circ \times 36^\circ$ resolution)
180 and ROCKGEM (Colbourn et al., 2013) modules, respectively.

Simulations start from pre-industrial spin-ups (Holden et al., 2013b) and follow historical transient forcing
from 850 to 2005 CE (Eby et al., 2013). In this setting, the land use change emissions start from 850 CE and
emissions from other sources including fossil fuels are introduced from 1750 CE. The historical forcing includes
CO₂ emissions, non-CO₂ radiative forcings, and land use changes, including both anthropogenic and natural
185 sources (volcanic eruptions and solar variability). In order to meld the spin using RCP2.6 at year 2005 with the
projected scenario SSP1-2.6, a constant adjustment of 0.446 Wm^{-2} was added to the non-CO₂ radiative forcing.
This adjustment can be viewed as representing contributions from land use change albedo (explicitly modelled in
GENIE-1, Fig. 1c) and from non-anthropogenic forcings, which were modelled in the historical spin-up (Eby et
al., 2013), comprising volcanic forcing of 0.184 Wm^{-2} , and solar forcing of 0.059 Wm^{-2} in 2005.

190 The future forcing scenario (2005 to 2420) follows SSP1-2.6 (Riahi et al., 2017) to the year 2100, and is
extended to 2420. Negative emissions are applied as a reduction in anthropogenic CO₂ emissions from the late
2020s, giving net negative emissions from 2077. To extend the SSP1-2.6 from 2100, we follow a similar protocol
to Meinshausen et al. (2020). Land-use change CO₂ emissions are reduced to zero by 2150 with non-CO₂ land-use
emissions held fixed from 2100. Fossil fuel emissions, including non-CO₂ greenhouse gases, and negative CO₂
195 emissions are all brought to zero by 2250 (Fig. 1a and c). This protocol differs slightly from Meinshausen et al.
(2020) who reduce negative emissions to zero by 2200; we prefer to avoid a second period of positive emissions
from 2200 to 2250. Therefore, we have three CO₂ emission phases: positive emissions from 2020 to 2077, net
negative emissions from 2077 to 2250 and zero emissions from 2250 to 2420 (Fig. 1a).

We assume that the carbon removed through negative emissions leaves the system permanently, which is the
200 representation of NETs with long-lived and permanent carbon storage such as carbon capture and storage. This
assumption also approximates enhanced rock weathering, although the chemical effects of weathering products
are neglected, such as the effect of bicarbonate changes on ocean biogeochemistry which drive co-benefits for the
ocean and marine ecosystems (Vakilifard et al., 2021).

205

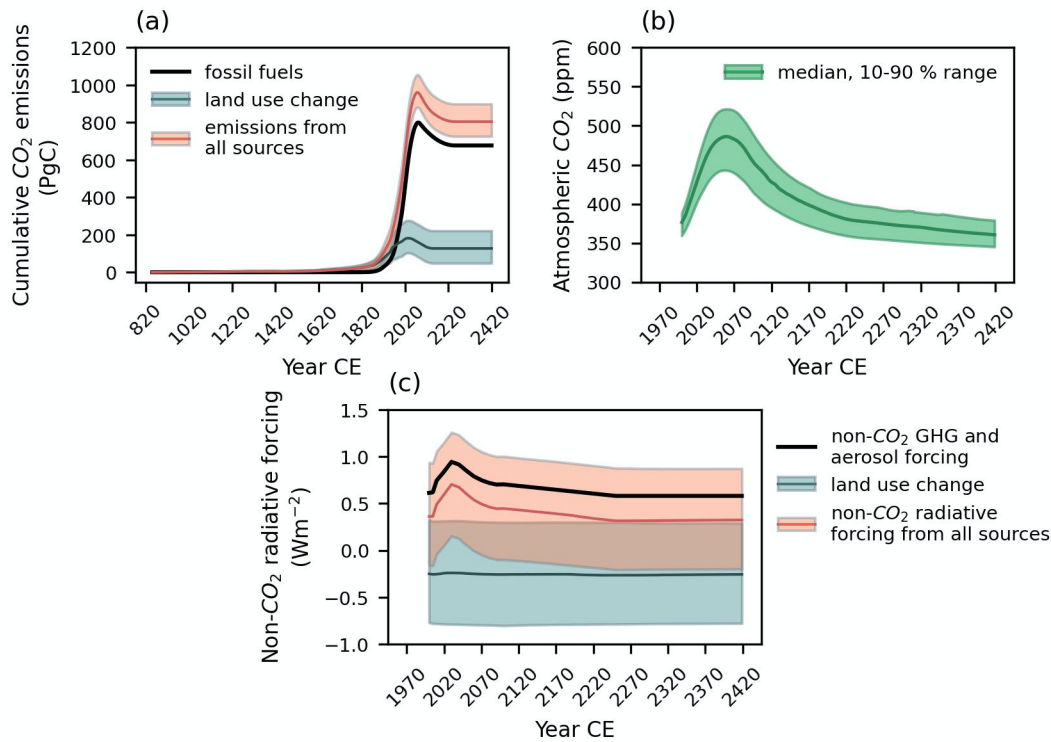


Figure 1: (a) The cumulative CO₂ emissions from 850 CE fill the end of the model integration at year 2420, (b) the evolution of the atmospheric CO₂ and (c) non-CO₂ radiative forcing from year 2000 for SSP1-2.6 scenario. Solid lines show the median values, and shaded areas indicate the values between the 10th and 90th percentiles.

210 To quantify the uncertainty in climate and carbon-cycle responses, we used an 86-member ensemble, a subset of a calibrated 471-member ensemble varying 28 model parameters (Holden et al., 2013a). The selection of 24 of these parameters (Holden et al., 2013b) covers oceanic, atmospheric, sea-ice, ocean biogeochemistry and terrestrial vegetation processes that are thought to contribute to variability of atmospheric CO₂ on glacial/interglacial timescales (Kohfeld and Ridgwell, 2009). The remaining four parameters are relevant to the modern state of the

215 climate carbon-cycle, describing uncertainties in soil under land management, crop albedo, climate sensitivity and CO₂ fertilization. The 86 ensemble members are perturbed to cover uncertainty in the 28 parameters and are all constrained to simulate plausible pre-industrial values of global temperature, Atlantic overturning circulation, sea ice coverage, vegetative and soil carbon, sedimentary calcium carbonate and dissolved ocean oxygen (Holden et al., 2013b). They additionally simulate reasonable values of atmospheric CO₂ at snapshots (1620, 1770, 1850,

220 1970 and 2005 CE) through the historical transient (Foley et al., 2016). The varied parameters are summarised in

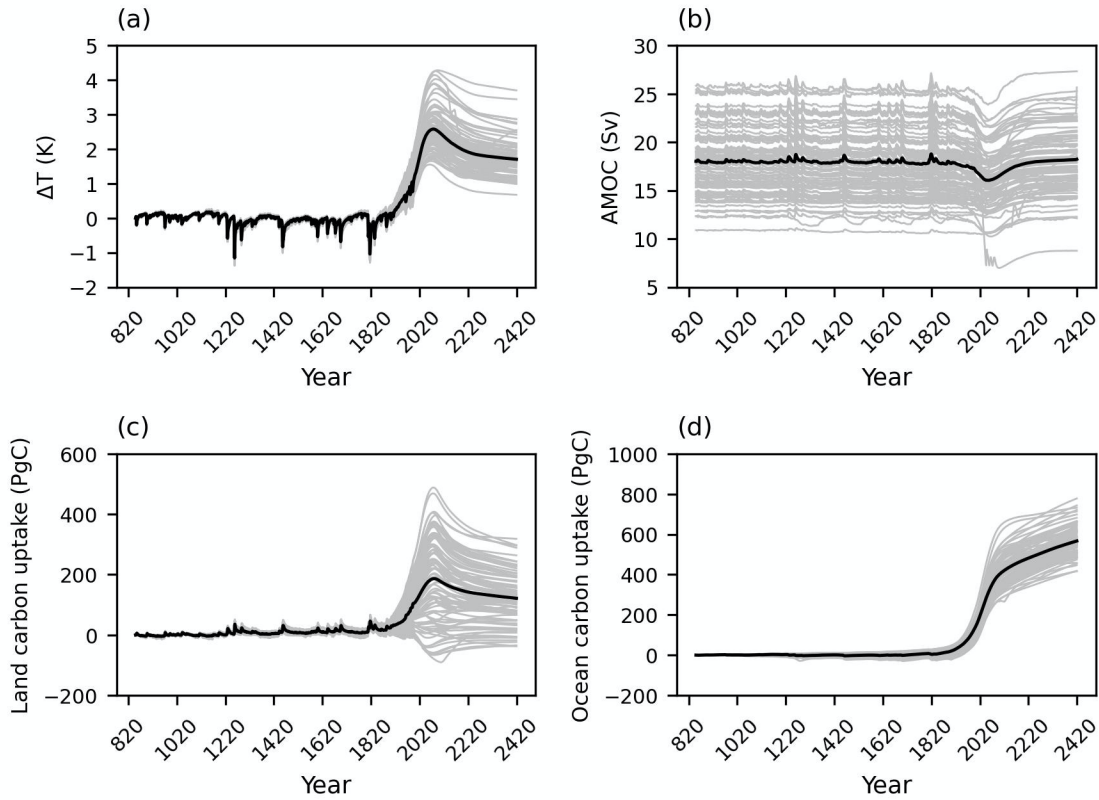
Supplementary Table 4 and are fully detailed, along with the ensemble design methodology, in Holden et al. (2013a and 2013b).

4 GENIE-1 model responses

The GENIE-1 model responses are next described in terms of the spread of ensemble responses, and the essentials
225 of the carbon and thermal responses.

4.1 Characterising the model ensemble

There are a wide range of responses within the ensemble members making up the model projections following the
future forcing scenario SSP1-2.6. At the end of the positive emission phase at year 2077, the increase in surface
air temperature ranges from 1.5 to 4.2 K, the Atlantic meridional overturning circulation change from -12.3 to 0.6
230 Sv, the land carbon change from a loss of 78 PgC to a gain of 488 PgC, and the ocean carbon uptake from a gain
of 247 to 586 PgC (Fig. 2).



235 **Figure 2: Inter-model spread of 86-member ensemble for change in (a) the surface air temperature, (b) Atlantic meridional overturning circulation (AMOC), (c) land carbon pool and (d) ocean carbon pool from year 850 CE until year 2420 following the SSP1-2.6 scenario. Black lines show the mean values.**

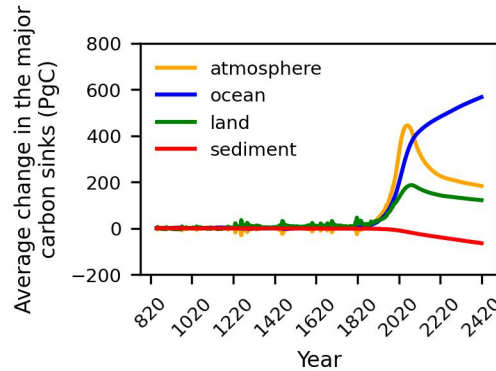
4.2 Carbon response

The distribution of carbon between carbon inventories is diagnosed (Fig. 3), and carbon conservation ensures that at all times the sum of the change in the carbon content of the atmosphere, $\Delta I_{atmos}(t)$, ocean, $\Delta I_{ocean}(t)$, land, 240 $\Delta I_{land}(t)$, and ocean sediment, $\Delta I_{sediment}(t)$, equals the cumulative CO₂ emissions from both land use change and fossil fuels, $I_{em}(t)$, with all inventories in PgC,

$$\Delta I_{atmos}(t) + \Delta I_{ocean}(t) + \Delta I_{land}(t) + \Delta I_{sediment}(t) = I_{em}(t) \quad (10)$$

Aside from the ocean sediments, which lose carbon, there is an increase in the carbon content of all inventories between the years 2020 and 2077, the positive emission phase (Fig. 3). During this emission phase, the carbon release from the sediment reservoir is ~ 14 PgC on average, equivalent to a sedimentary CaCO₃ dissolution flux 245 of ~ 21 TmolC yr⁻¹ consistent with Archer (1996), Ridgwell and Hargreaves (2007) and Sulpis et al. (2018). The application of carbon capture and storage from year 2077 decreases the total carbon inventory until year 2250.

During the zero emission phase, the increase in ocean storage is associated with a decrease in carbon content in the atmosphere, land and sediment.



250

Figure 3: The ensemble average change in the major carbon inventories from 850 CE until year 2420 for SSP1-2.6 scenario.

4.3 Thermal response

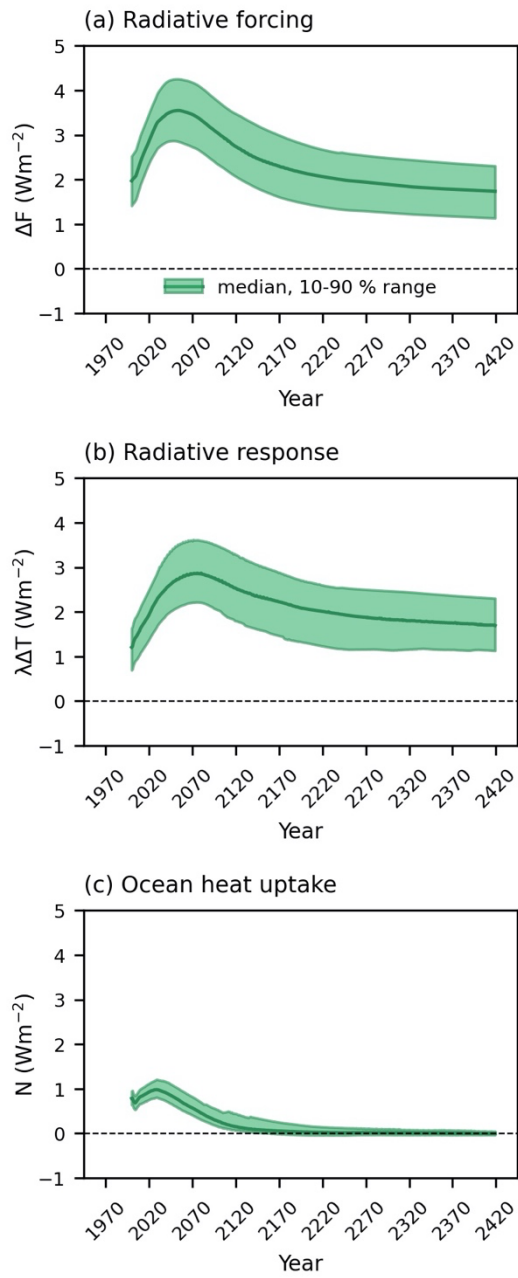
For the thermal analysis, a global energy balance (Eq. 5) is diagnosed, $\Delta F(t) = N(t) + \lambda(t)\Delta T(t)$, in which the energy balance is expressed as the relationship between radiative forcing, $\Delta F(t)$ (Wm^{-2}), planetary heat uptake, $N(t)$ (Wm^{-2}) and radiative response, $\lambda(t)\Delta T(t)$ (Wm^{-2}).

The radiative forcing, $\Delta F(t)$, is the sum of non- CO_2 radiative forcing (including land use change albedo) and CO_2 radiative forcing. The non- CO_2 radiative forcing, $\Delta F_{non-\text{CO}_2}(t)$ (Wm^{-2}) is a prescribed model forcing input, besides land use change which is diagnosed as the change in reflected surface insolation under land use change relative to that with natural vegetation, averaged annually across all grid cells. The land use change maps were also fixed from year 2005 and these were associated with a global forcing of -0.53 to 0.05 Wm^{-2} (25th to 75th percentile range) and mean and median values of -0.23 and -0.26 Wm^{-2} , respectively, across the ensemble. The uncertainty is driven primarily by crop albedo which varies between 0.12 and 0.18 across the ensemble (Holden et al., 2013a). The CO_2 radiative forcing, $\Delta F_{\text{CO}_2}(t)$ (Wm^{-2}), was calculated individually for each simulation based on the atmospheric CO_2 concentration ($C(t)$ (ppm)) as outlined in IPCC (2001):

$$\Delta F_{\text{CO}_2}(t) = \alpha \ln \left(\frac{C(t)}{C(t_0)} \right) \quad (11)$$

265 where α is a constant equal to 5.35 Wm^{-2} and $C(t_0)$ equals 278 ppm.

The ocean heat uptake is used to represent the planetary heat uptake, as the model ocean is the principal energy sink and the model does not take into account the energy stored in the lithosphere or consumed in the melting of the ice sheets. In comparison, in real world, the ocean is responsible for storing over 90 % of the Earth's total energy increase (Church et al., 2011). The climate feedback parameter, $\lambda(t)$ ($\text{K}^{-1} (\text{Wm}^{-2})$), is diagnosed from
270 the ocean heat uptake and the change in global-mean, surface air temperature (Eq. 5). Most of the radiative forcing drives a radiative response involving a rise in surface air temperature, rather than an increase in ocean heat uptake (Fig. 4).



275 **Figure 4: The evolution of (a) radiative forcing, (b) radiative response and (c) ocean heat uptake in SSP1-2.6 scenario from year 2000. Solid lines show the median values and shaded areas indicate the values between the 10th and 90th percentiles.**

5 Model responses in terms of climate metrics

The climate response of the GENIE-1 model projections for positive and negative emissions are next assessed in terms of the response of two climate metrics, the effective Transient Climate Response to Emissions (eTCRE) and the effective Zero Emissions Commitment (eZEC), as well as identifying the asymmetrical response to positive and negative emissions.

The results of GENIE-1 simulations show a linear relationship between the change in the surface air temperature and cumulative CO₂ emissions over the positive emission phases (Fig. 5), with the slopes of this relationship varying between ~ 1.62 and 3.42 K EgC⁻¹ (based on the 10 % and 90 % percentile values). The range of slopes of the ΔT versus I_{em} curve, calculated by linear regression, over the net negative emission phase is larger than in the positive emission phase by a factor of ~ 2 due to decrease in non-CO₂ radiative forcing leading to additional cooling during this period. Over this emission phase, the warming relationship is not linear in all ensemble members, and exhibits a hysteresis behaviour, as previously identified in Zickfeld et al. (2016), Jeltsch-Thömmes et al. (2020) and Koven et al. (2022). Differences in the rates of surface air temperature change over the net negative emission phase are mainly due to the terrestrial carbon uncertainty (discussed in Sect. 4.2.2).

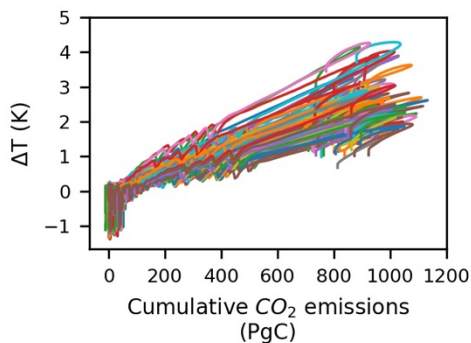


Figure 5: Change in the surface air temperature versus cumulative CO₂ emissions from 850 CE until year 2420 in SSP1-2.6 scenario.

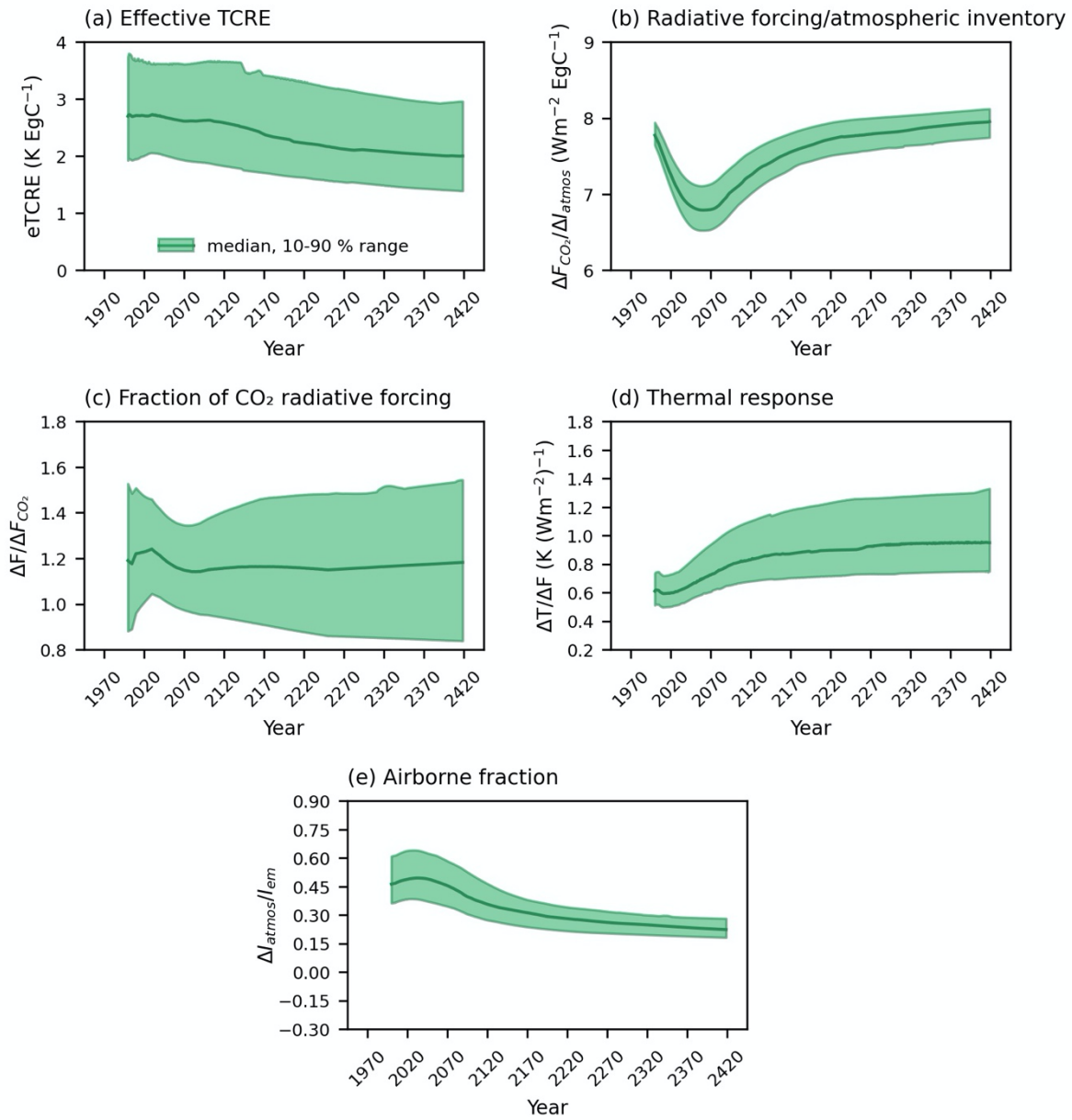
5.1 Drivers of the effective Transient Climate Response to Emissions

Following Sect. 2, the effective Transient Climate Response to Emissions (eTCRE) is evaluated in terms of the product of (i) the dependence of surface warming on the radiative forcing, referred to as the thermal dependence, $\Delta T(t)/\Delta F(t)$; (ii) the dependence of the radiative forcing on the cumulative CO₂ emissions, referred to as a radiative dependence, $\Delta F(t)/\Delta I_{atmos}(t)$; and (iii) the airborne fraction, $\Delta I_{atmos}(t)/I_{em}(t)$, referred to as a carbon dependence (Eq. 9):

$$300 \quad eTCRE \equiv \frac{\Delta T(t)}{I_{em}(t)} = \underbrace{\left(\frac{\Delta T(t)}{\Delta F(t)}\right)}_{thermal} \underbrace{\left(\frac{\Delta F(t)}{\Delta F_{CO_2}(t)}\right)}_{radiative \text{ from } CO_2 \text{ and non-}CO_2} \underbrace{\left(\frac{\Delta F_{CO_2}(t)}{\Delta I_{atmos}(t)}\right)}_{carbon} \underbrace{\left(\frac{\Delta I_{atmos}(t)}{I_{em}(t)}\right)}_{carbon}.$$

The model ensemble reveals a decrease in eTCRE from the median value of 2.71 K EgC⁻¹ in year 2020 to 2.0 K EgC⁻¹ in year 2420 (with 10-90 % range of 2.0 to 3.65 and 1.39 to 2.96 K EgC⁻¹, respectively) (Fig. 6a). During the positive emission phase (to year 2077) this reduction is driven by a weakening the radiative forcing with an increase in atmospheric carbon (Fig. 6b), which dominates over the increase in the thermal dependence (Fig. 6d).
 305 During the net negative and zero emission phases (from year 2077), the eTCRE reduction is driven by the reducing airborne fraction as CO₂ is drawn down by the ocean (Fig. 6e).

The eTCRE is scenario dependent and varies with both CO₂ and non-CO₂ portions of the radiative forcing. Following the analysis of Matthews et al. (2021), we quantify the spread of the non-CO₂ fraction of total anthropogenic forcing, f_{nc} (from Eq. 8), between 2020 and 2100 (Table S1) to investigate the extent of scenario
 310 dependency of the eTCRE. The results show that f_{nc} range varies from ~ 10 % to ~ 26 % (25 %-75 % percentile values) in 2020 to ~ 5 % to ~ 21 % in 2100, corresponding to ~ 6 % decrease (mean value) over the course of 80 years. The TCRE diagnosed by removing the non-CO₂ warming factor (from Eq. 8) remains constant at ~ 2.2 K EgC⁻¹ (median values) over the entire period. However, the uncertainty increases towards the end of the century varying from 1.75 to 2.82 K EgC⁻¹ (10 % -90 % percentile values) in 2020 to up to ~ 3.13 K EgC⁻¹ in 2100
 315 (Fig. S1).



320 **Figure 6: Effective transient climate response to the cumulative CO_2 emissions (eTCRE) and its components for SSP1-2.6 scenario from year 2000. (a) eTCRE, (b) dependence of the radiative forcing on atmospheric CO_2 , (c) fractional radiative forcing contribution from atmospheric CO_2 , (d) airborne fraction and (e) thermal dependence. Solid lines show the median values, and shaded areas indicate the values between the 10th and 90th percentiles.**

The uncertainty in the eTCRE, and its dependencies for the model ensemble, is assessed based on the non-dimensional coefficient of variation, given by the inter-model standard deviation divided by the ensemble mean
 325 (Williams et al., 2020). The uncertainty in the eTCRE varies from 0.23 to 0.3 over the course of the model

integrations and is larger by 0.05 for the net negative emission phase compared to the positive emission phase (Table 1).

330 During the positive and net negative emissions, the coefficients of variation for the thermal dependence (~ 0.18 to ~ 0.2) and airborne fraction (~ 0.2) provide the dominant contributions to the eTCRE uncertainty (Table 1). During the zero emission phase, however, the coefficient of variation for the fractional radiative forcing contribution from atmospheric CO₂, $\Delta F(t)/\Delta F_{CO_2}(t)$ (~ 0.22), is larger than the contribution from the airborne fraction (~ 0.16). In all emission phases, the dependence of the radiative forcing on atmospheric CO₂, $\Delta F_{CO_2}(t)/\Delta I_{atmos}(t)$, has the least contribution to the eTCRE uncertainty (~ 0.02).

335 **Table 1: Effective transient climate response to the cumulative CO₂ emissions (eTCRE) and its components for the different emission phases in the SSP1-2.6 scenario. The coefficient of variation (σ_x/\bar{x}) is defined by the inter-model standard deviation (σ_x) divided by the inter-model mean (\bar{x}).**

Variable	2020-2077			2077-2250			2250-2420		
	\bar{x}	σ_x	σ_x/\bar{x}	\bar{x}	σ_x	σ_x/\bar{x}	\bar{x}	σ_x	σ_x/\bar{x}
I _{em} (PgC)	855.29	72.63	0.08	856.45	72.63	0.08	806.38	72.63	0.09
ΔT (K)	2.33	0.51	0.22	2.17	0.59	0.27	1.77	0.55	0.31
eTCRE (K EgC ⁻¹)	2.74	0.63	0.23	2.54	0.71	0.28	2.20	0.67	0.30
$\Delta T/\Delta F$ (K (Wm ⁻²) ⁻¹)	0.68	0.12	0.18	0.89	0.18	0.20	0.97	0.22	0.23
λ^{-1} (K (Wm ⁻²) ⁻¹)	0.92	0.22	0.24	1.01	0.41	0.41	1.04	0.38	0.37
1-N/ ΔF	0.75	0.06	0.08	0.93	0.11	0.12	0.97	0.12	0.12
$\Delta I_{atmos}/I_{em}$	0.49	0.10	0.20	0.33	0.07	0.21	0.25	0.04	0.16
$\Delta F/\Delta F_{CO_2}$	1.20	0.14	0.12	1.18	0.20	0.17	1.19	0.26	0.22
$\Delta F_{CO_2}/I_{atmos}$ (Wm ⁻² EgC ⁻¹)	6.91	0.21	0.03	7.45	0.19	0.03	7.86	0.15	0.02

5.1.1 Carbon dependence for the effective Transient Climate Response to Emissions

The fraction of emitted CO₂ that remains in each carbon inventory (based on Eq. 7) varies over the course of the integrations. The carbon dependence for the eTCRE is given by the airborne fraction of carbon emissions, 340 $\Delta I_{atmos}(t)/I_{em}(t)$. By the year 2077, the end of the positive emission phase, the atmosphere is the largest carbon

sink with airborne fraction of $\sim 49\%$ (mean value) (Fig. 7a and Table S2). After year 2077, during the net negative and zero emission phases, the ocean becomes the dominant carbon sink with an increase in the ocean-borne fraction, $\Delta I_{ocean}(t)/I_{em}(t)$, up to $\sim 67\%$ (mean value) by 2420 (Fig. 7b and Table S2). The land-borne fraction, $\Delta I_{land}(t)/I_{em}(t)$ decreases from $\sim 19\%$ (mean value) in 2020 to the minimum value of $\sim 15\%$ in 2420 (Fig. 7c and Table S2). The sediment-borne fraction, $\Delta I_{sediment}(t)/I_{em}(t)$, remains negative at ~ -0.04 (mean value) over the entire period (Fig. 7d and Table S2), and therefore acts as a weak carbon source.

The coefficient of variation is the largest for the land-borne fraction (~ 0.7), followed by the sediment-borne fraction (~ -0.5) and then the airborne and ocean-borne fractions decreasing from ~ 0.2 over the positive emission phase to ~ 0.15 during the zero emission phase (Table S2). The main contribution to the model ensemble spread is, therefore, the land carbon system.

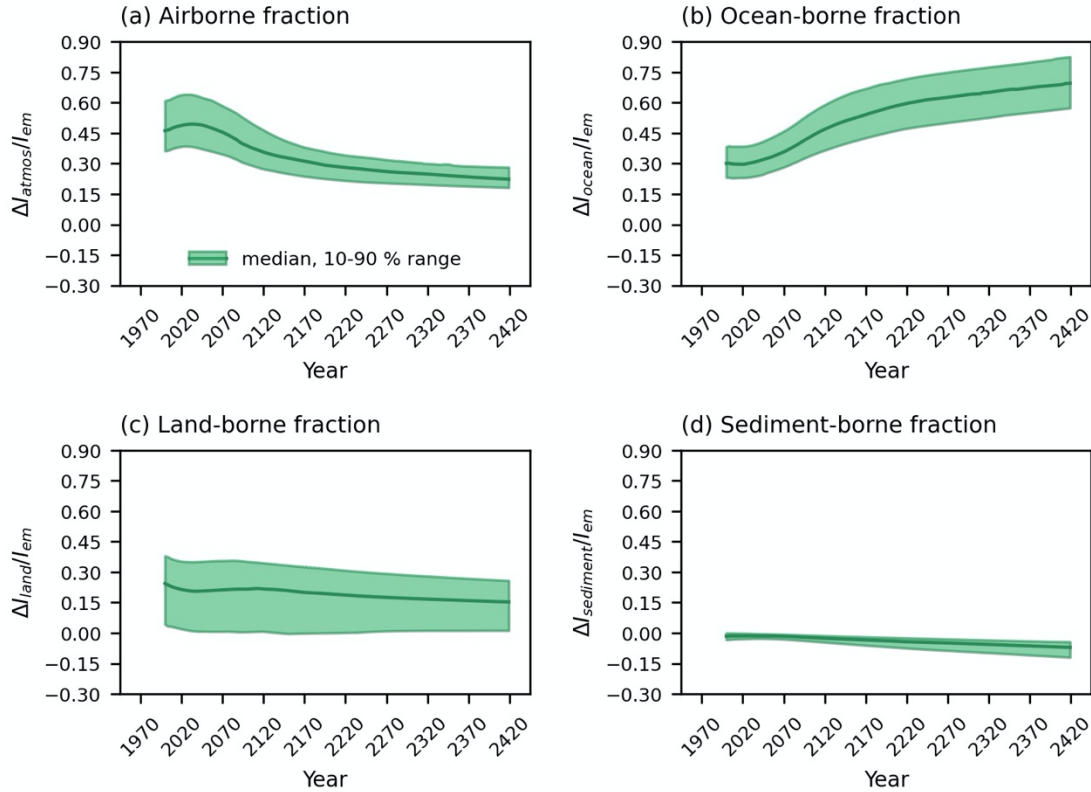
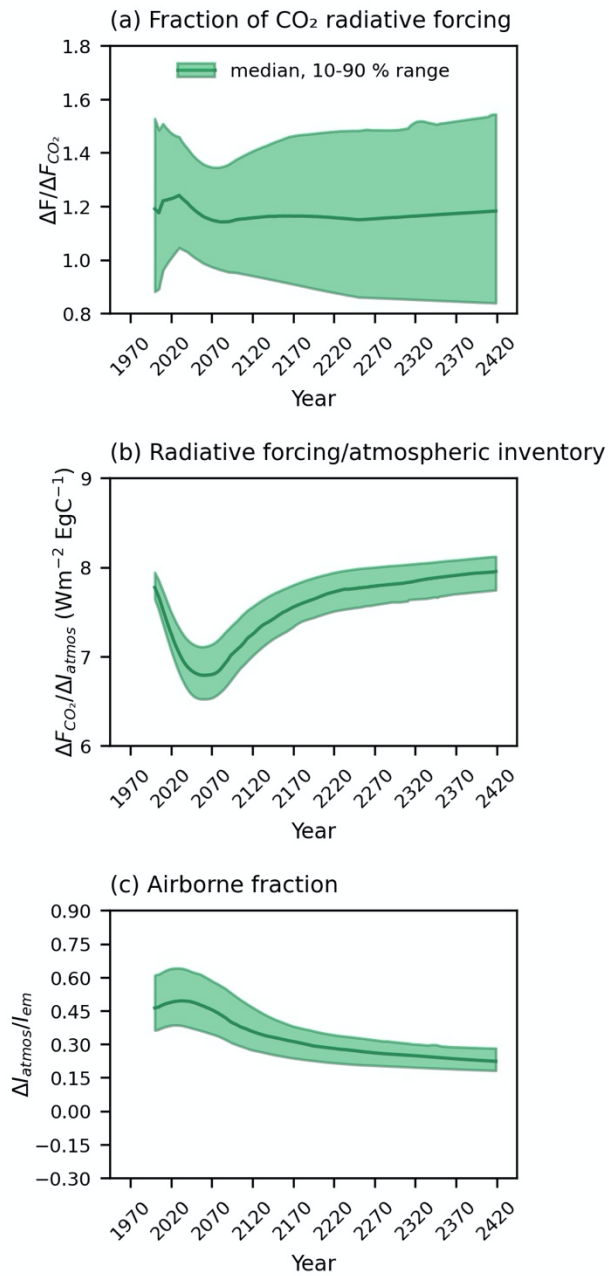


Figure 7: The evolution of (a) airborne fraction, (b) ocean-borne fraction, (c) land-borne fraction and (d) sediment-borne fraction in SSP1-2.6 scenario. Note that the y-axis shows the cumulative fraction of CO₂ which remains in each carbon inventory. Solid lines show the median values, and shaded areas indicate the values between the 10th and 90th percentiles from year 2000.

355 **5.1.2 Radiative forcing dependence for the effective Transient Climate Response to Emissions**

By the end of the positive emissions at year 2077, the radiative forcing dependence on atmospheric CO₂ emissions, $\Delta F(t)/\Delta I_{atmos}(t)$, weakens due to a saturation in the radiative forcing with an increase in atmospheric CO₂ (Gillett et al., 2013; William et al., 2020) (Fig. 1b and Fig. 8b). During the net negative emissions and zero emission phases over the next few centuries from year 2077 onwards, $\Delta F(t)/\Delta I_{atmos}(t)$ rises again due to a decrease in
360 atmospheric CO₂ associated with the decrease in the airborne fraction (Fig. 8c).

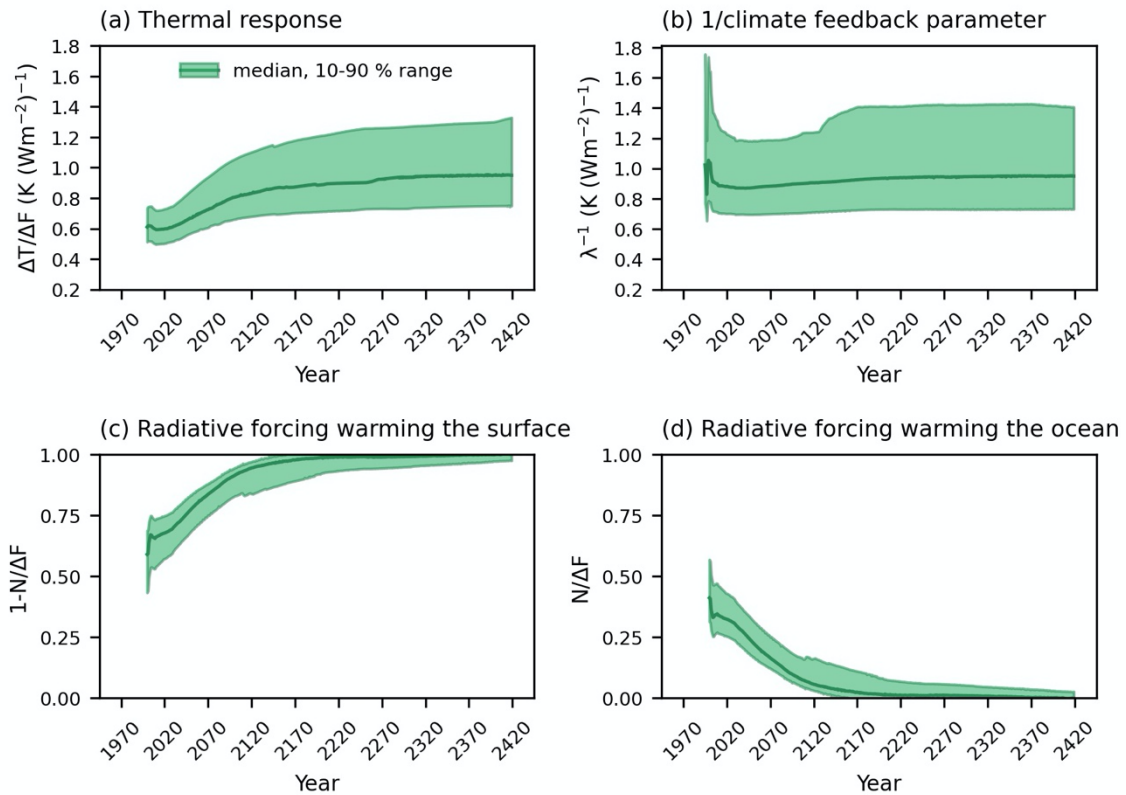


365 **Figure 8: Radiative forcing dependence for the effective TCRE and its components in SSP1-2.6 scenario from year 2000. (a) Fractional radiative forcing contribution from atmospheric CO₂, (b) dependence of the radiative forcing on atmospheric CO₂ and (c) airborne fraction. Solid lines show the median values, and shaded areas indicate the values between the 10th and 90th percentiles.**

5.1.3 Thermal dependence for the effective Transient Climate Response to Emissions

The thermal dependence of the eTCRE, involving the dependence of the surface warming on the radiative forcing, $\Delta T(t)/\Delta F(t)$, increases in all emission phases (Fig. 9a) due to the reinforcing contributions of the inverse of the climate feedback parameter, $\lambda(t)^{-1}$ (Fig. 9b) and the fraction of the radiative forcing warming the surface, $1 - N(t)/\Delta F(t)$ (Fig. 9c). The increase in $\lambda(t)^{-1}$ is equivalent to a slight decrease in the climate feedback $\lambda(t)$. The temporal evolution of the climate feedback parameter is mirrored in other climate model studies as climate feedbacks evolve on different timescales according to the nature of the controlling processes (Gregory et al., 2004; Armour et al., 2013; Knutti and Rugenstein, 2015; Goodwin, 2018). The fraction of the radiative forcing warming the surface increases by $\sim 22\%$ (based on the mean values, Table 1) from years 2020 to 2420 and with a corresponding reduction in the heat transfer into the deep ocean; by year 2420, nearly all the radiative forcing is warming the surface with the ratio $1 - N(t)/\Delta F(t)$ reaching 0.97 (mean values, Table 1) (Fig. 9c-d). This response is probably due to an increase in ocean stratification from the rise in surface ocean temperature (Figs. S2-S4) from the increased radiative forcing.

The coefficient of variation for the thermal dependence remains ~ 0.2 over the entire period (Table 1). Within the thermal dependence, the term relating to the climate feedback parameter $\lambda(t)^{-1}$ has a coefficient of variation more than ~ 3 times that of the fraction of the radiative forcing warming the surface $1 - N(t)/\Delta F(t)$ (Table 1). As the thermal dependence terms, $\lambda(t)^{-1}$ and $1 - N(t)/\Delta F(t)$, are strongly anti-correlated (Fig. S5), the relative spread in the thermal response is thus mitigated by the feedback between the climate feedback parameter and the fraction of the radiative forcing warming the surface.



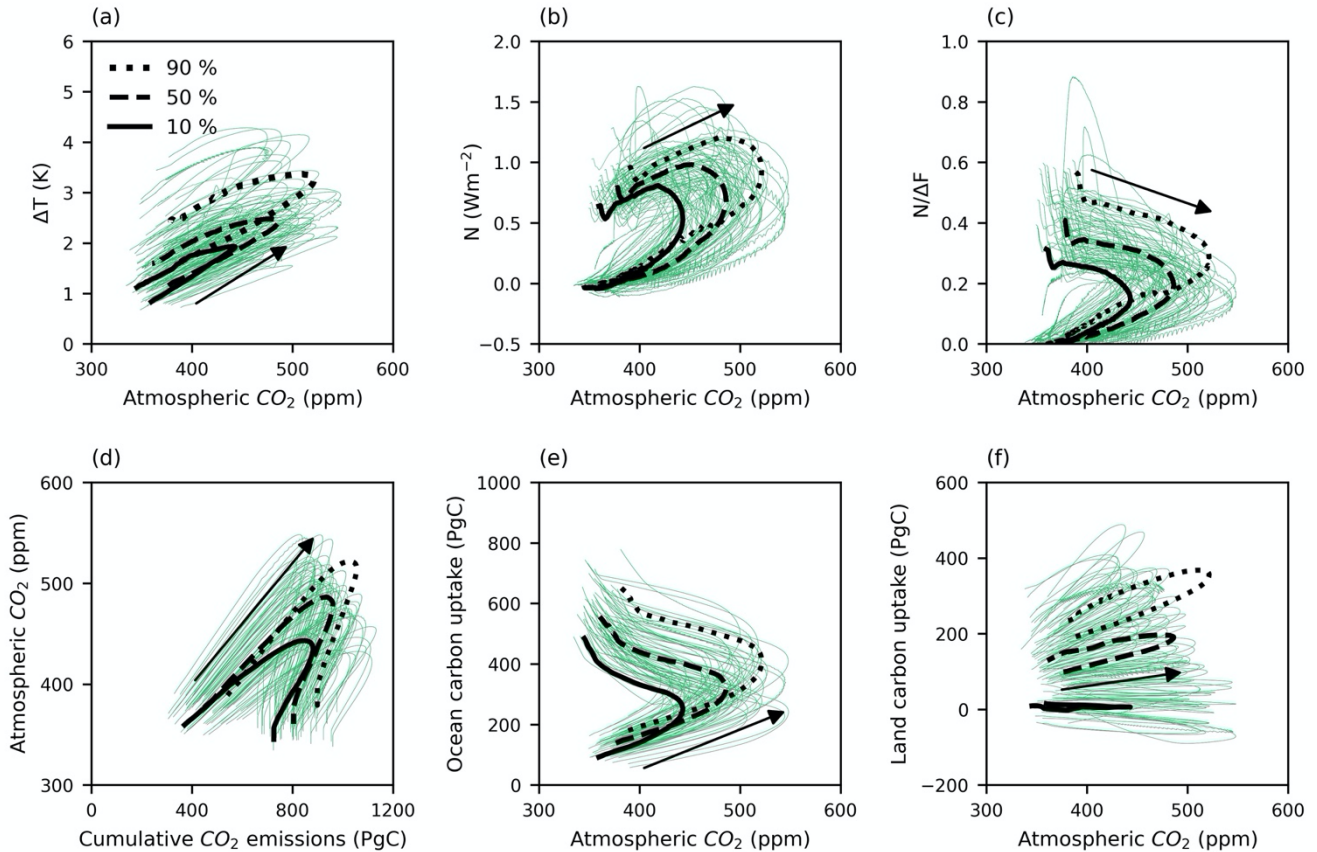
390 **Figure 9: The evolution of (a) thermal dependence for the effective TCRE given by the dependence of the surface warming on the radiative forcing, $\Delta T(t)/\Delta F(t)$, and the contributions from (b) the inverse of the climate feedback, (c) the fraction of the radiative forcing warming the surface and (d) the fraction of the radiative forcing warming the ocean interior in SSP1-2.6 scenario from year 2000. Solid lines show the median values, and shaded areas indicate the values between the 10th and 90th percentiles.**

5.2 The asymmetry of the Earth system response to positive and negative emissions

5.2.1 Hysteresis

The relationship between the surface air temperature and atmospheric CO₂ exhibits hysteresis behaviour in most ensemble members, consistent with climate change reversibility studies (Fig. 10a) (Tokarska and Zickfeld, 2015; 395 Jeltsch-Thömmes et al., 2020). The temperature remains at high levels after high atmospheric CO₂ concurrent with a decrease in the ocean heat uptake, $N(t)$ (Fig. 10b). The ability of the ocean interior in taking up heat diminishes in time, probably due to increasing stratification and weakening ventilation. The fraction of the radiative forcing warming the ocean interior, $N(t)/\Delta F(t)$ (Fig. 10c) then continues to decrease after the peak in atmospheric CO₂ leading to higher surface air temperatures even after the lower CO₂ concentrations are restored.

400 The atmospheric CO₂ declines during the net negative emission phase from year 2077 (Fig. 1b) (associated with the cumulative CO₂ emissions of ~ 960.4 PgC (median value) (Figs. 1a and 10d). After the cessation of the emissions, the atmospheric CO₂ continues to decrease (Fig. 10d) mainly due to uptake by the ocean and to a lesser extent the land (Fig. 10e-f). The ocean carbon uptake is governed by the air-sea flux of CO₂ and thermocline ventilation, with uncertainties dominated by ventilation processes transferring carbon from the surface ocean to
405 the main thermocline and deep ocean (Holden et al., 2013b; Goodwin et al., 2015; Zickfeld et al., 2016; Jeltsch-Thömmes et al., 2020). The ocean continues to take up carbon after the peak in atmospheric CO₂ as there is continuing long-term adjustment and ventilation of the deep ocean (Fig. 10e). The complex responses of land carbon (Fig. 10f) are driven by a range of competing processes, most notably carbon uptake through CO₂ fertilization and the carbon release through historical land use changes and accelerated respiration under warming.



415

Figure 10: The thermal (upper row) and carbon (lower row) variables versus atmospheric CO₂ in SSP1-2.6 scenario from year 2000. (a) Change in surface air temperature; (b) ocean heat uptake; and (c) fraction of the radiative forcing warming the ocean interior; (d) cumulative CO₂ emissions; (e) change in the ocean carbon pool; and (f) change in the land carbon pool. In each panel the black lines show the median, 10th and 90th percentile values of the atmospheric CO₂ versus the median, 10th and 90th percentile values of the thermal and carbon variables.

5.2.2 Correlation between the model parameters and the slope of the change in surface air temperature versus cumulative CO₂ emissions ($\Delta T/\Delta I_{em}$)

We calculated the coefficients of determination (R^2) between $\Delta T/\Delta I_{em}$ and the 28 model parameters across the ensemble during both positive and net negative emission phases. For this purpose, four of the 86 simulations were omitted as outliers because they were undergoing substantial re-organisation of ocean circulation during the period of net negative emissions (Fig. S6), significantly perturbing ocean heat uptake.

During the positive emission phase, uncertainty in $\Delta T/\Delta I_{em}$ is dominated by the radiative feedback parameter (OL1) ($R^2 \sim 61\%$) (Table 2), which perturbs outgoing longwave radiation proportionally to ΔT (Matthews and

425 Caldeira, 2007). This parameter is primarily designed to capture unmodelled cloud responses to global average temperature change, and it has previously been shown to drive 81 % of the variance in GENIE-1 climate sensitivity (Holden et al., 2010). The parameter links to the climate feedback parameter in the eTCRE framework (Sect. 4.1) which was shown to be the dominant driver of uncertainty in the thermal response and therefore eTCRE values.

430 Although radiative forcing uncertainty dominates, carbon-cycle parameters also drive $\Delta T/\Delta I_{em}$ variance via the land use change soil carbon parameter (KC) ($R^2 \sim 12\%$) through its control on soil carbon losses under land use change. The fractional vegetation parameter (VFC) ($R^2 \sim 11\%$) drives additional carbon-cycle uncertainty through its control on terrestrial carbon surface density. The results are associated with the airborne fraction in the eTCRE framework diagnosed as another factor controlling the uncertainty in eTCRE during this emission phase (Sect. 4.1).

435 During net negative emissions (2077-2250), uncertainty in $\Delta T/\Delta I_{em}$ is affected mainly by the CO₂ fertilisation (VPC) ($R^2 \sim 35\%$) which is a major source of terrestrial carbon uncertainty and to a lesser extent the parameter that controls the rate of carbon loss from soils under land use change (KC, $\sim 11\%$). The effect of the carbon contribution in the uncertainty is expressed through airborne fraction in the eTCRE framework, which was revealed to be the main reason behind the large spread of eTCRE over the net negative emission phase (Sect. 4.1),
 440 consistent with MacDougall et al. (2017).

Table 2: Correlation between model parameters and $\Delta T/\Delta I_{em}$ in SSP1-2.6 scenario over different emission phases based on the coefficients of determination (R^2) (%). $R^2 > 50\%$ denotes strong correlation, and $R^2 > 10\%$ moderate correlation. The values less than 10 % are shown in Table S3.

Emission phase	Parameter	Description	Coefficient of determination (R^2) (%)
2020-2077	OL1	Radiative feedback parameter ($W\ m^{-2}$)	61.4
	KC	Land use change soil carbon	11.7
	VFC	Fractional vegetation dependence on vegetation carbon density ($m^2\ kgC^{-1}$)	10.9
2077-2250	VPC	CO ₂ fertilisation (ppm)	34.9
	KC	Land use change soil carbon	11.2

445

5.3 The effective Zero Emissions Commitment

The zero emissions commitment (ZEC) is now assessed given by the mean surface air temperature change after CO₂ emissions cease (Hare and Meinshausen, 2006; Matthews and Caldeira, 2008, Froelicher and Paynter, 2015; MacDougall et al., 2020). Whether there is continued surface warming depends on a competition between a cooling
450 effect from reduction in atmospheric CO₂ due to the ocean and land sequestration of carbon versus a surface warming effect from a decline in the heat uptake by the ocean interior (Williams et al., 2017b).

In our analysis, we define the effective ZEC (eZEC), which assesses the continued surface warming after the cessation of CO₂ emissions while the non-CO₂ greenhouse gases and aerosol forcings evolve. Our reference scenario applies SSP1-2.6 CO₂ emissions until year 2077 and zero emissions thereafter, with cumulative emissions
455 of ~ 961 PgC (median value) (Fig. S7). Following the analysis of MacDougall et al. (2020), we define eZEC₂₅, eZEC₅₀, eZEC₉₀ as the mean surface air temperature anomalies at the 25th, 50th and 90th years after the cessation of emissions, to account for the implications of eZEC over a range of multi-decadal timescales relevant to climate policy.

Diagnosed eZEC values are illustrated in Fig. 11 (the reference plotted as orange bars). In the reference
460 scenario, the distribution of the eZEC display an uncertain sign. There is a temperature overshoot in 20 % of eZEC₂₅ values (10-90 % range from -0.08 to 0.02 K) and in 11 % of eZEC₅₀ values (range from -0.17 to 0.01 K) and 5 % of eZEC₉₀ values (range from -0.31 to -0.05 K). The ensemble means of eZEC₂₅, eZEC₅₀ and eZEC₉₀ are -0.03, -0.10 and -0.21 K, respectively, and compare to values of -0.01, -0.07 and -0.12 K in the 1000 PgC experiment of MacDougall et al. (2020) (grey bars). The additional cooling is in part due to ongoing reductions of
465 non-CO₂ forcing from 0.728 Wm⁻² in 2077 to 0.648 Wm⁻² in 2167 (Fig. 1c), noting that MacDougall et al. (2020) performed an idealised experiment that only considered CO₂ emissions forcing. We realise that our uncertainties are lower than MacDougall et al. (2020), which at least in part reflects the absence of internal (decadal) variability in the EMBM of GENIE-1, noting that inter-annual, but not decadal, variability was removed from MacDougall et al. (2020) through 20-year averaging.

In contrast to the reference scenario, surface temperatures decrease in all the ensemble members after
470 cessation of positive emissions in SSP1-2.6 scenario. We consider two alternative interpretations of the eZEC, the warming after the cessation of positive emissions (in 2077) and the warming after the cessation of net negative emissions (in 2250). The former may be more relevant from a policy perspective (as the time of likely peak warming), while the latter is theoretically useful to quantify committed warming when emissions are precisely
475 zero.

The blue bars in Fig. 11 illustrate the eZEC results for SSP1-2.6 scenario calculated relative to 2250. There is a temperature overshoot in 5 % of the eZEC₂₅ values, however, the values remain at or below zero within 10-90 % range (-0.06 to 0 K). The values of eZEC₂₅ and eZEC₉₀ are robustly negative, ranging from -0.1 to -0.01 K and -0.16 to -0.03 K (10th-90th percentile range), respectively. Ensemble means are -0.03 K for eZEC₂₅,
480 -0.06 K for eZEC₅₀ and -0.09 K for eZEC₉₀.

The green bars in Fig. 11 illustrate the eZEC values from 2077 (which includes the period of ongoing net negative emissions). The average values of eZEC are significantly lower than from 2250, being -0.1, -0.26, and -0.47 K, due to the additional cooling driven by net negative emissions. All eZEC values are again robustly negative, varying between -0.14 and -0.05 for eZEC₂₅, -0.34 and -0.16 for eZEC₅₀, and -0.61 and -0.31 for eZEC₉₀
485 (10 % -90 % percentile values), confirming that no ensemble member exhibits a temperature overshoot after the cessation of positive emissions.

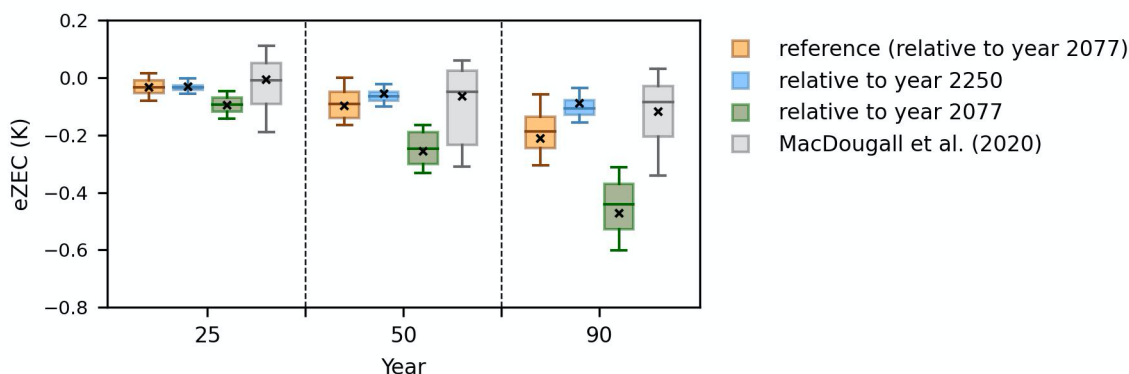


Figure 11: The distribution of the effective zero emissions commitment (eZEC) in the reference scenario at 25th, 50th and 90th years relative to year 2077 (orange bars) and in SSP1-2.6 relative to year 2250 (blue bars) and relative to year 2077 (green bars) versus the zero emissions commitment results of MacDougall et al. (2020) (grey bars). The mean values are shown with cross marks. Note that the year 2077 is the end of the positive emission phase, and the year 2250 is the end of the net negative emission phase.
490

6 Conclusions

There is an increasing need to develop and implement carbon capture and sequestration techniques to meet the
495 Paris agreement 1.5 °C and 2 °C temperature targets (UNFCCC, 2015). However, it is unclear how these negative emissions affect the climate response, as represented by two key climate metrics: the effective Transient Climate Response to Emissions (eTCRE), defining the relationship between surface warming and cumulative CO₂ emissions, and the effective Zero Emissions Commitment (eZEC), defining the anticipated warming after the

cessation of CO₂ emissions and continued non-CO₂ greenhouse gases and aerosol forcings. The effect of negative
500 emissions is assessed here using a GENIE-1 ensemble, following SSP1-2.6 with the net negative CO₂ emissions
of ~ 156 PgC over 173 years. The model responses include 86 members that span a wide range of climate and
carbon-cycle feedback strengths. The ensemble analysis is enabled by employing low resolution and intermediate
complexity, with most notable simplifications of the fixed wind-field energy-moisture balance atmosphere,
neglecting dynamic atmosphere-ocean feedbacks, and the simple model of terrestrial carbon, which neglects
505 nutrient limitation, does not represent permafrost (or methane), and has a 1-level description of soil carbon.

The eTCRE decreases in time due to a combination of the weakening in the radiative forcing with an increase
in atmospheric carbon during positive emissions and with a reduction in the airborne fraction after emissions cease,
which together outweigh the strengthening thermal dependence.

The comparison of the coefficient of variation for the eTCRE and its dependencies show that the thermal
510 dependence and airborne fraction almost equally contribute to the uncertainty in the eTCRE during the positive
emission phase. The results are consistent with those from the model parameter correlation analysis in which
different slopes of the change in surface air temperature versus emissions are due to primarily to the uncertainty
in radiative feedbacks and to a lesser extent carbon-cycle feedbacks. Our results differ from the analysis of CIMIP5
and CMIP6 ensembles in which the radiative forcing response and thermal response were the main contributors to
515 the uncertainty in the TCRE, respectively (Williams et al., 2020). During the net negative emission phase, both
analyses show that the carbon dependence causes the main uncertainty in the values of eTCRE.

The relationship between thermal and carbon feedbacks with an increase in atmospheric CO₂ exhibits
hysteresis behaviour. The fraction of the radiative forcing warming the surface continues to increase after peak
atmospheric CO₂ as the ocean is stratified, leading to higher surface air temperatures after lower atmospheric CO₂
520 values are restored. The increase in the ocean storage after the peak in atmospheric CO₂ is associated with the
long-term adjustment and ventilation of the deep ocean while the reason for the continued terrestrial carbon storage
relates to competing processes such as carbon uptake through CO₂ fertilization and carbon release through
historical land use changes and accelerated respiration under warming.

The eZEC is close to zero. In the model mean of the integrations that exclude carbon capture and storage, the
525 eZEC is -0.03 K at 25 years and decreases to -0.21 K at 90 years after emissions cease. However, even assisted by
gradual reductions in non-CO₂ forcing as in this scenario, the distribution of eZEC after 25 years from the cessation
of emissions shows continued warming in ~ 20 % of ensemble members. Including carbon capture and storage
reduces the probability of continued warming after net zero, with 95 % ensemble members exhibiting an eZEC

close to or below zero. Hence, implementing negative emissions is required to reduce the risk of overshoot and
530 continued warming after net zero is reached and increase the probability of meeting the Paris targets. NETs with
naturally long CO₂ removal lifetimes, such as enhanced rock weathering (Beerling et al., 2020) may be especially
well suited for this purpose as the legacy effects of the repeated application of this technology increase the rate of
carbon drawdown per unit area for years after implementation at no incremental cost (Beerling et al., 2020;
Vakilifard et al., 2021).

535 *Data availability.* The data that support the findings of this study are available from the corresponding author upon reasonable request.

Author contributions. NV undertook model experimental design, all simulations, and analyses. All authors were involved in the design of the model experiments, led by NV and RGW. All authors contributed to writing, led by
540 NV and RGW.

Competing interests. The authors declare that they have no conflict of interest.

Acknowledgments. The authors acknowledge funding with a Leverhulme Research Centre Award, RC-2015-029,
545 from the Leverhulme Trust. RGW is supported by a UK Natural Environment Research Council grant NE/T007788/1.

References

- Archer, D.: A data-driven model of the global calcite lysocline, *Global Biogeochem. Cy.*, 10, 511 – 526, doi: 10.1029/96GB01521, 1996.
- 550 Armour, K. C., Bitz, C. M., and Roe, G. H.: Time-varying climate sensitivity from regional feedbacks, *J. Clim.*, 26, 4518-4534, doi: 10.1175/JCLI-D-12-00544.1, 2013.
- Beerling, D. J., Kantzas, E. P., Lomas, M. R., Wade, P., Eufrazio, R. M., Renforth, P., Sarkar, B., Andrews, M. G., James, R. H., Pearce, C. R., Mercure, J. F., Pollitt, H., Holden, P. B., Edwards, N. R., Khanna, M., Koh, L., Quegan, S., Pidgeon, N. F., Janssens, I. A., Hansen, J., and Banwart, S. A.: Potential for large-scale CO₂ removal via enhanced rock weathering
555 with croplands, *Nature*, 583, 242–248, doi: 10.1038/s41586-020-2448-9, 2020.
- Boucher, O., Halloran, P. R., Bruke, E. J., Doutriaux-Boucher, M., Jones, C. D., Lowe, J., Ringer, M. A., Robertson, E., and Wu, P.: Reversibility in an Earth System model in response to CO₂ concentration changes, *Environ. Res. Lett.*, 7, 024013, doi:10.1088/1748-9326/7/2/024013, 2012.
- Church, J. A., White, N. J., Konikow, L. F., Domingues, C. M., Cogley, J. G., and Rignot, E., Gregory, J. M., van den Broeke, M. R., Monaghan, A. J., and Velicogna, I.: Revisiting the Earth's sea-level and energy budgets from 1961 to
560 2008, *Geophys. Res. Lett.*, 38, L18601, doi:10.1029/2011GL048794, 2011.
- Colbourn, G., Ridgwell, A., and Lenton, T. M.: The rock geochemical model (RokGeM) v0.9, *Geosci. Model Dev.*, 6, 1543–1573, doi: 10.5194/gmd-6-1543-2013, 2013.

- Eby, M., Weaver, A. J., Alexander, K., Zickfeld, K., Abe-Ouchi, A., Cimatoribus, A. A., Crespin, E., Drijfhout, S. S., Edwards, N. R., Eliseev, A. V., Feulner, G., Fichefet, T., Forest, C. E., Goosse, H., Holden, P. B., Joos, F., Kawamiya, M., Kicklighter, D., Kienert, H., Matsumoto, K., Mokhov, I. I., Monier, E., Olsen, S. M., Pedersen, J. O. P., Perrette, M., Philippon-Berthier, G., Ridgwell, A., Schlosser, A., Schneider von Deimling, T., Shaffer, G., Smith, R. S., Spahni, R., Sokolov, A. P., Steinacher, M., Tachiiri, K., Tokos, K., Yoshimori, M., Zeng, N., and Zhao, F.: Historical and idealized climate model experiments: an intercomparison of Earth system models of intermediate complexity, *Clim. Past*, 9, 1111–1140, doi: 10.5194/cp-9-1111-2013, 2013.
- Edwards N. R., and Marsh R.: Uncertainties due to transport-parameter sensitivity in an efficient 3-D ocean-climate model, *Clim. Dyn.*, 24, 415–433, doi:10.1007/s00382-004-0508-8, 2005.
- Ehlert, D., Zickfeld, K., Eby, M., and Gillett, N.: The sensitivity of the proportionality between temperature change and cumulative CO₂ emissions to ocean mixing, *J. Clim.*, 30, 2921–2935, doi: 10.1175/JCLI-D-16-0247.1, 2017.
- Foley, A. M., Holden, P. B., Edwards, N. R., Mercure, J.-F., Salas, P., Pollitt, H. and Chewpreecha, U.: Climate model emulation in an integrated assessment framework: A case study for mitigation policies in the electricity sector, *Earth Syst. Dyn.*, 7, 119–132, doi: 10.5194/esd-7-119-2016, 2016.
- Forster, P. M., Andrews, T., Good, P., Gregory, J. M., Jackson, L. S., and Zelinka, M.: Evaluating adjusted forcing and model spread for historical and future scenarios in the CMIP5 generation of climate models, *J. Geophys. Res. Atmos.*, 118, 1139–1150, doi: 10.1002/jgrd.50174, 2013.
- Froelicher, T. L., and Paynter, D. J.: Extending the relationship between global warming and cumulative carbon emissions to multi-millennial timescales, *Environ. Res. Lett.*, 10, 075002, doi: 10.1088/1748-9326/10/7/075002, 2015.
- Friedlingstein, P., Andrew, R. M., Rogelj, J., Peters, G. P., Canadell, J. G., Knutti, R., Luderer, G., Raupach, M. R., Schaeffer, M., van Vuuren, D. P., and Le Quéré, C.: Persistent growth of CO₂ emissions and implications for reaching climate targets, *Nature Geosci.*, 7, 709–715, doi: 10.1038/ngeo2248, 2014.
- Gillett, N. P., Arora, V. K., Matthews, D., and Allen, M. R.: Constraining the ratio of global warming to cumulative carbon emissions using CMIP5 simulations, *J. Clim.*, 26, 6844–6858, doi: 10.1175/JCLI-D-12-00476.1, 2013.
- Goodwin, P., Williams, R. G., and Ridgwell, A.: Sensitivity of climate to cumulative carbon emissions due to compensation of ocean heat and carbon uptake, *Nat. Geosci.*, 8, 29–34, doi: 10.1038/ngeo2304, 2015.
- Goodwin, P.: On the time evolution of climate sensitivity and future warming, *Earth’s Fut.*, 6, 1336–1348, doi: 10.1029/2018EF000889, 2018.
- Gregory, J. M., Ingram, W. J., Palmer, M. A., Jones, G. S., Stott, P. A., Thorpe, R. B., Lowe, J. A., Johns, T. C., and Williams, K. D.: A new method for diagnosing radiative forcing and climate sensitivity, *Geophys. Res. Lett.*, 31, L03205, doi: 10.1029/2003GL018747, 2004.
- Hare, B., and Meinshausen, M.: How much warming are we committed to and how much can be avoided?, *Clim. Change*, 75, 111–149, doi: 10.1007/s10584-005-9027-9, 2006.

- Holden, P. B., Edwards, N. R., Oliver, K. I. C., Lenton, T. M., and Wilkinson, R. D.: A probabilistic calibration of climate sensitivity and terrestrial carbon change in GENIE-1, *Clim. Dyn.*, 35, 785–806, doi: 10.1007/s00382-009-0630-8, 2010.
- Holden, P. B., Edwards, N. R., Gerten, D., and Schaphoff, S.: A model-based constraint on CO₂ fertilisation, *Biogeosciences*, 600 10, 339–355, doi: 10.5194/bg-10-339-2013, 2013a.
- Holden, P. B., Edwards, N. R., Müller, S. A., Oliver, K. I. C., Death, R. M., and Ridgwell, A.: Controls on the spatial distribution of oceanic $\delta^{13}\text{C}_{\text{DIC}}$, *Biogeosciences*, 10, 1815–1833, doi: 10.5194/bg-10-1815-2013, 2013b.
- Intergovernment Panel on Climate Change (IPCC), *Climate change 2001: The scientific basis*. Cambridge, UK: Cambridge University Press, 2001.
- 605 Intergovernment Panel on Climate Change (IPCC), *Climate change 2013: The physical science basis*. Cambridge, UK: Cambridge University Press, 2013.
- Intergovernment Panel on Climate Change (IPCC), *Climate change 2021: The scientific basis*. Cambridge, UK: Cambridge University Press, 2021.
- Jeltsch-Thömmes, A., Stocker, T. F., and Joos, F.: Hysteresis of the Earth system under positive and negative CO₂ 610 emissions, *Environ. Res. Lett.*, 15, 124026, doi: 10.1088/1748-9326/abc4af, 2020.
- Jones, C., Robertson, E., Arora, V., Friedlingstein, P., Shevliakova, E., Bopp, L., Brovkin, V., Hajima, T., Kato, E., Kawamiya, M., Liddicoat, S., Lindsay, K., Reick, C. H., Roelandt, C., Segschneider, J., and Tjiputra, J.: Twenty-first-century compatible CO₂ emissions and airborne fraction simulated by CMIP5 Earth system models under four representative concentration pathways, *J. Clim.*, 26, 4398–4413, doi: 10.1175/JCLI-D-12-00554.1, 2013.
- 615 Jones, C. D., and Friedlingstein, P.: Quantifying process-level uncertainty contributions to TCRE and carbon budgets for meeting Paris Agreement climate targets, *Environ. Res. Lett.*, 15, 074019, doi: 10.1088/1748-9326/ab858a, 2020.
- Katavouta, A., Williams, R. G., Goodwin, P., and Roussenov, V.: Reconciling atmospheric and oceanic views of the transient climate response to emissions, *Geophys. Res. Lett.* 45, 6205–6214, doi: 10.1029/2018GL077849, 2018.
- Knutti, R., and Rugenstein, M. A. A.: Feedbacks, climate sensitivity and the limits of linear models, *Phil. Trans. Royal Soc.* 620 A, 373, doi: 10.1098/rsta.2015.0146, 2015.
- Koch, A., Brierley, C., Maslin, M. M., and Lewis, S. L.: Earth system impacts of the European arrival and Great Dying in the Americas after 1492. *Quat. Sci. Rev.*, 207,13-36, doi: 10.1016/j.quascirev.2018.12.004, 2019.
- Kohfeld, K. E., and Ridgwell, A.: Glacial-interglacial variability in atmospheric pCO₂, in *Surface Ocean-Lower Atmosphere Processes*, *Geophys. Res. Ser.*, 187, 251–286, doi:10.1029/2008GM000845, 2009.
- 625 Koven, C. D., Arora, V. K., Cadule, P., Fisher, R. A., Jones, C. D., Lawrence, D. M., Lewis, J., Lindsay, K., Mathesius S., Meinshausen, M., Mills, M., Nicholls, Z., Sanderson, B. M., Séférian, R., Swart, N. C., Wieder, W. R., and Zickfeld, K.: Multi-century dynamics of the climate and carbon cycle under both high and net negative emissions scenarios, *Earth Syst. Dyn.*, 13, 885-909, doi: 10.5194/esd-13-885-2022, 2022.

- Luderer, G., Pietzcker, R. C., Bertram, C., Kriegler, E., Meinshausen, M., and Edenhofer, O.: Economic mitigation challenges: how further delay closes the door for achieving climate targets, *Environ. Res. Lett.*, 8, 034033, doi: 10.1088/1748-9326/8/3/034033, 2013.
- MacDougall, A. H: The transient response to cumulative CO₂ emissions: a review, *Curr. Clim. Change Rep.*, 2, 39–47, doi: 10.1007/s40641-015-0030-6, 2016.
- MacDougall, A. H., Swart, N. C., and Knutti, R.: The uncertainty in the transient climate response to cumulative CO₂ emissions arising from the uncertainty in physical climate parameters, *J. Clim.*, 30, 813-27, doi: 10.1175/JCLI-D-16-0205.1, 2017.
- MacDougall, A. H., Frölicher, T.L., Jones, C. D., Rogelj, J., Matthews, H. D., Zickfeld, K., Arora, V. K., Barrett, N. J., Brovkin, V., Burger, F. A., Eby, M., Eliseev, A. V., Hajima, T., Holden, P. B., Jeltsch-Thömmes, A., Koven, C., Mengis, N., Menviel, L., Michou, M., Mokhov, I. I., Oka, A., Schwinger, J., Séférian, R., Shaffer, G., Sokolov, A., Tachiiri, K., Tjiputra, J., Wiltshire, A., and Ziehn, T.: Is there warming in the pipeline? A multi-model analysis of the zero emissions commitment from CO₂, *Biogeosciences*, 17, 2987-3016, doi: 10.5194/bg-17-2987-2020, 2020.
- Matthews, H. D., and Caldeira, K.: Transient climate–carbon simulations of planetary geoengineering, *Proc. Natl Acad. Sci.*, 104, 9949-9954, doi: 10.1073/pnas.0700419104, 2007.
- Matthews, H. D., and Caldeira, K.: Stabilizing climate requires near–zero emissions, *Geophys. Res. Lett.*, 35, L04705, doi: 10.1029/2007GL032388, 2008.
- Matthews, H. D., Gillett, N. P., Stott, P. A., and Zickfeld, K.: The proportionality of global warming to cumulative carbon emissions, *Nature*, 459, 829–832, doi: 10.1038/nature08047, 2009.
- Matthews, H. D., and Zickfeld, K.: Climate response to zeroed emissions of greenhouse gases and aerosols, *Nat. Clim. Change*, 2, 338-341, doi: 10.1038/nclimate1424, 2012.
- Matthews, H. D., Landry, J. S., Partanen, A. I., Allen, M., Eby, M., Forster, P. M., Friedlingstein, P., and Zickfeld, K.: Estimating carbon budgets for ambitious climate targets, *Curr. Clim. Change Rep.*, 3, 69-77, doi: 10.1007/s40641-017-0055-0, 2017.
- Matthews, H. D., Zickfeld, K., Knutti, R., and Allen, M. R.: Focus on cumulative emissions, global carbon budgets and the implications for climate mitigation targets, *Environ. Res. Lett.*, 13, 010201, doi: 10.1088/1748-9326/aa98c9, 2018.
- Matthews, H. D., Tokarska, K. B., Rogelj, J., Smith, C., MacDougall, A. H., Haustein, K., Mengis, N., Sippel, S., Forster, P. M., and Knutti, R.: An integrated approach to quantifying uncertainties in the remaining carbon budget, *Commun. Earth Environ.*, 2, 7, doi: 10.1038/s43247-020-00064-9, 2021.
- Meinshausen, M., Nicholls, Z. R. J., Lewis, J., Gidden, M. J., Vogel, E., Freund, M., Beyerle, U., Gessner, C., Nauels, A., Bauer, N., Canadell, J. G., Daniel, J. S., John, A., Krummel, P. B., Luderer, G., Meinshausen, N., Montzka, S. A., Rayner, P. J., Reimann, S., Smith, S. J., van den Berg, M., Velders, G. J. M., Vollmer, M. K., and Wang, R. H. J.: The

- shared socio-economic pathway (SSP) greenhouse gas concentrations and their extensions to 2500, *Geosci. Model Dev.*, 13, 3571–3605, doi: 10.5194/gmd-13-3571-2020, 2020.
- O'Neill, B.C., Kriegler, E., Ebi, K.L., Kemp-Benedict, E., Riahi, K., Rothman, D.S., van Ruijven, B.J., van Vuuren, D.P., Birkmann, J., Kok, K., and Levy, M.: The roads ahead: Narratives for shared socioeconomic pathways describing world
665 futures in the 21st century, *Glob. Environ. Change*, 42, 169-180, doi: 10.1016/j.gloenvcha.2015.01.004, 2017.
- Riahi, K., van Vuuren, D. P., Kriegler, E., Edmonds, J., O'Neill, B. C., Fujimori, S., Bauer, N., Calvin, K., Dellink, R., Fricko, O., Lutz, W., Popp, A., Cuaresma, J. C., Samir, K.C., Leimbach, M., Jiang, L., Kram, T., Rao, S., Emmerling, J., Ebi, K., Hasegawa, T., Havlík, P., Humpenöder, F., Da Silva, L. A., Smith, S., Stehfest, E., Bosetti, V., Eom, J., Gernaat, D., Masui, T., Rogelj, J., Strefler, J., Drouet, L., Krey, V., Luderer, G., Harmsen, M., Takahashi, K., Baumstark, L., Doelman,
670 J. C., Kainuma, M., Klimont, Z., Marangoni, G., Lotze-Campen, H., Obersteiner, M., Tabeau, A., and Tavoni, M.: The Shared Socioeconomic Pathways and their energy, land use, and greenhouse gas emissions implications: An overview, *Glob. Environ. Change*, 42, 153-168, doi: 110.1016/j.gloenvcha.2016.05.009, 2017.
- Ridgwell, A., and Hargreaves, J. C.: Regulation of atmospheric CO₂ by deep-sea sediments in an Earth system model. *Global Biogeochem. Cy.*, 21, doi: 10.1029/2006GB002764, 2007.
- 675 Ridgwell, A., Hargreaves, J. C., Edwards, N. R., Annan, J. D., Lenton, T. M., Marsh, R., Yool, A., and Watson, A.: Marine geochemical data assimilation in an efficient Earth System Model of global biogeochemical cycling, *Biogeosciences*, 4, 87–104, doi:10.5194/bg-4-87-2007, 2007.
- Rogelj, J., Luderer, G., Pietzcker, R. C., Kriegler, E., Schaeffer, M., Krey, V., and Riahi, K.: Energy system transformations for limiting end-of-century warming to below 1.5 °C, *Nat. Clim. Change*, 5, 519–27, doi: 10.1038/nclimate2572, 2015.
- 680 Solomon, S., Plattner, G. K., Knutti, R., and Friedlingstein, P.: Irreversible climate change due to carbon dioxide emissions, *Proc. Natl. Acad. Sci. USA*, 106, 1704–1709, doi: 10.1073/pnas.0812721106, 2009.
- Spafford, L., and MacDougall, A. H.: Quantifying the probability distribution function of the transient climate response to cumulative CO₂ emissions, *Environ. Res. Lett.*, 15, 034044, doi: 10.1088/1748-9326/ab6d7b, 2020.
- Sulpis, O., Boudreau, B. P., Mucci, A., Jenkins, C., Trossman, D. S., Arbic, B. K., and Key, R. M.: Current CaCO₃ dissolution
685 at the seafloor caused by anthropogenic CO₂, *Proc. Natl. Acad. Sci. U. S. A.*, 115, 11700-11705, doi: 10.1073/pnas.1804250115, 2018.
- Tokarska, K. B., and Zickfeld, K.: The effectiveness of net negative carbon dioxide emissions in reversing anthropogenic climate change, *Environ. Res. Lett.*, 10, 094013, doi: 10.1088/1748-9326/10/9/094013, 2015.
- Tokarska, K. B., Gillet, N. P., Arora, V. K., Lee, W. G., and Zickfeld, K.: The influence of non-CO₂ forcings on cumulative
690 carbon emissions budgets, *Environ. Res. Lett.*, 13, doi: 10.1088/1748-9326/aaafdd, 2018.
- United Nations Framework Convention on Climate Change (UNFCCC): Adoption of the Paris Agreement, 21st Conference of the Parties, United Nations, Paris, 2015.

- Vakilifard, N., Kantzas, E. P., Holden, P. B., Edwards, N. R., and Beerling, D. J.: The role of enhanced rock weathering deployment with agriculture in limiting future warming and protecting coral reefs, *Environ. Res. Lett.*, 16, 094005, doi: 10.1088/1748-9326/ac1818, 2021.
- 695
- Williams, R. G., Goodwin, P., Roussenov, V. M., and Bopp, L.: A framework to understand the transient climate response to emissions, *Environ. Res. Lett.*, 11, 015003, doi: 10.1088/1748-9326/11/1/015003, 2016.
- Williams, R. G., Roussenov, V., Goodwin, P., Resplandy, L., and Bopp, L.: Sensitivity of global warming to carbon emissions: effects of heat and carbon uptake in a suite of Earth system models, *J. Clim.* 30 9343–63, doi: 10.1175/JCLI-D-16-0468.1, 700 2017.
- Williams, R. G., Roussenov, V., Frölicher, T. L., and Goodwin, P.: Drivers of continued surface warming after cessation of carbon emissions, *Geophys. Res. Lett.*, 44, 10633–10642, doi: 10.1002/2017GL075080, 2017b.
- Williams, R. G., Ceppi, P., and Katavouta, A.: Controls of the transient climate response to emissions by physical feedbacks, heat uptake and carbon cycling, *Environ. Res. Lett.*, 15, 0940c1, doi: 10.1088/1748-9326/ab97c9, 2020.
- 705 Zickfeld, K., Arora, V. K., and Gillett, N. P.: Is the climate response to CO₂ emissions path dependent?, *Geophys. Res. Lett.*, 39, L05703, doi: 10.1029/2011GL050205, 2012.
- Zickfeld, K., Eby, M., Weaver, A. J., Alexander, K., Cressin, E., Edwards, N. R., Eliseev, A. V., Feulner, G., Fichet, T., Forest, C. E., Friedlingstein, P., Goosse, H., Holden, P. B., Joos, F., Kawamiya, M., Kicklighter, D., Kienert, H., Matsumoto, K., Mikhov, I., Monier, E., Olsen, A. M., Pedersen, J. O. P., Perrette, M., Philippon-Berthier, G., Ridgwell, 710 A., Schlosser, A., Schneider Von Deimling, T., Shaffer, G., Sokolov, A., Spahni, R., Steinacher, M., Tachiiri, K., Tokos, K. S., Yoshimori, M., Zeng, N., and Zhao, F.: Long-term climate change commitment and reversibility: An EMIC intercomparison, *J. Clim.*, 26, 5782–5809, doi: 10.1175/JCLI-D-12-00584.1, 2013.
- Zickfeld, K., MacDougall, A. H., and Matthews, H. D.: On the proportionality between global temperature change and cumulative CO₂ emissions during periods of net negative CO₂ emissions, *Environ. Res. Lett.*, 11, 055006, doi: 715 10.1088/1748-9326/11/5/055006, 2016.